Blue-Shifted A–H Stretching Modes and Cooperative Hydrogen Bonding. 1. Complexes of Substituted Formaldehyde with Cyclic Hydrogen Fluoride and Water Clusters

ARTICLE *in* THE JOURNAL OF PHYSICAL CHEMISTRY A · SEPTEMBER 2007

Impact Factor: 2.69 · DOI: 10.1021/jp072717f · Source: PubMed

2 AUTHORS:

Alfred Karpfen
University of Vienna
162 PUBLICATIONS **4,284** CITATIONS
SEE PROFILE

Eugene S Kryachko
University of Liège
139 PUBLICATIONS **2,031** CITATIONS
SEE PROFILE

Blue-Shifted A−H Stretching Modes and Cooperative Hydrogen Bonding. 1. Complexes of Substituted Formaldehyde with Cyclic Hydrogen Fluoride and Water Clusters

Alfred Karpfen*,† and Eugene S. Kryachko*,‡

Institute for Theoretical Chemistry, University of Vienna, Währinger Strasse 17, A-1090 Vienna, Austria, and Department of Chemistry, Bat. B6c, University of Liege, Sart-Tilman, B-4000 Liege 1, Belgium, and Bogoliubov Institute for Theoretical Physics, Kiev, 03143 Ukraine

Received: April 6, 2007; In Final Form: June 13, 2007

The structures and vibrational spectra of the intermolecular complexes formed by insertion of substituted formaldehyde molecules HRCO (R = H, Li, F, Cl) into cyclic hydrogen fluoride and water clusters are studied at the MP2/aug-cc-pVTZ computational level. Depending on the nature of the substituent R, the cluster type, and its size, the C−H stretching modes of HRCO undergo large blue and partly red shifts, whereas all the F−H and O−H stretching modes of the conventional hydrogen bonds are strongly red-shifted. It is shown that (i) the mechanism of blue shifting can be explained within the concept of the negative intramolecular coupling between C−H and C═O bonds that is inherent to the HRCO monomers, (ii) the blue shifts also occur even if no hydrogen bond is formed, and (iii) variation of the acceptor X or the strength of the C−H···X hydrogen bond may either amplify the blue shift or cause a transition from blue shift to red shift. These findings are illustrated by means of intra- and intermolecular scans of the potential energy surfaces. The performance of the negative intramolecular coupling between C−H and C═O bonds of H_2CO is interpreted in terms of the NBO analysis of the isolated H_2CO molecule and H_2CO interacting with $(H_2O)_n$ and $(HF)_n$ clusters.

1. Introduction

Nearly a decade ago the classical hydrogen bonding theory has been partly extended to include so-called "improper" or "blue-shifting hydrogen bonds".[1−3] The latter sharply contrast with what was our common perception of classical or conventional hydrogen bonds laid down for almost a century and in fact belong to a broader class of so-called "weak hydrogen bonds".[4−6] The area of blue-shifting hydrogen (or shortly H) bonds was initially unveiled by those of the C−H···X type, which demonstrate the contraction of the C−H bond, a concomitant blue shift of the stretching vibrational mode ν(C−H), the decrease of its infrared intensity, and also the apparent absence of a direct relationship, typical for the conventional ones, between the hydrogen bonding interaction energy and the magnitude of the blue shift.[1−3]

Several theoretical models, based on the charge-transfer natural bond orbital analysis,[7−12] the interplay of hyperconjugation and rehybridization,[13] the energy decomposition scheme,[11] the repulsive (Pauli) steric interactions,[12] and the modeling of the formation of the C−H···Y hydrogen bond via embedding into a homogeneous electric field,[13−16] have been invoked to rationalize the blue-shifting mechanism.

In the recent series of computational studies, we have attempted to enlarge the class of conceivable blue-shifting hydrogen bonds by investigating cyclic complexes formed by the insertion of a guest molecule into cyclic hydrogen fluoride clusters $(HF)_m$ ($1 \le m \le 3$). Fluoromethanes, CH_nF_{4-n} ($1 \le n \le 3$),[17] and alternative proton donors such as fluorophosphines,[16b] fluoroarsines,[16b] fluorosilanes,[18] and formaldehyde[16a] have been chosen as the guest molecule (the latter is symbolically designated as H_kX-A where, e.g., X = CF_{3-n} in CH_nF_{4-n} and X = C in H_2CO, A = F in CH_nF_{4-n} and A = O in H_2CO). Some of these complexes exhibit rather large C−H blue shifts falling into the range 50−120 cm^{-1}.

These investigations[16−19] have provided solid computational evidence that the origin of such large blue shifts in cyclic hydrogen-bonded clusters mainly stems from the following three conditions: (i) the existence of a dominant conventional hydrogen bond X−A···H−F, in which the guest molecule plays the role of the proton acceptor, (ii) the simultaneous existence of the blue-shifting hydrogen bond A−X−H···F, in which the guest molecule acts as the proton donor, and (iii) the existence of a negative intramolecular coupling (NIC) between the X−A and H−X bonds of the isolated guest molecule H_kX-A. This feature, which implies that the H−X bond responds "negatively", i.e., contracts, to an elongation of the X−A bond, can be treated as the force-field manifestation of the general negative intramolecular response effect that particularly governs the well-known negative hyperconjugative interaction.[20] The performance of the NIC is particularly striking in numerous well-known dimeric complexes where the guest molecule acts solely as proton acceptor, and hence its X−H (or C−H as in fluoromethanes and formaldehyde) bonds are not involved in hydrogen bonding (see, e.g., refs 2, 3, 6f, 16−19, and 21). Among them are particularly the complexes formed between dimethyl ether and H_2O, hydrogen−halides HX (X = F, Cl, Br), and dihalogens XY (X, Y = F, Cl, Br), which, as recently demonstrated,[19b] exhibit blue shifts of the C−H stretching frequencies, although the CH_3 groups are not directly involved in the formation of an intermolecular bond. This theoretical

* Corresponding authors. A.K.: fax, +43 1 4277 9527; e-mail: alfred.karpfen@univie.ac.at. E.S.K.: fax, +32 4 366 3413; e-mail: eugene.kryachko@ulg.ac.be.

† University of Vienna.

‡ University of Liege and Bogoliubov Institute for Theoretical Physics.

10.1021/jp072717f CCC: $37.00
Published on Web 07/28/2007

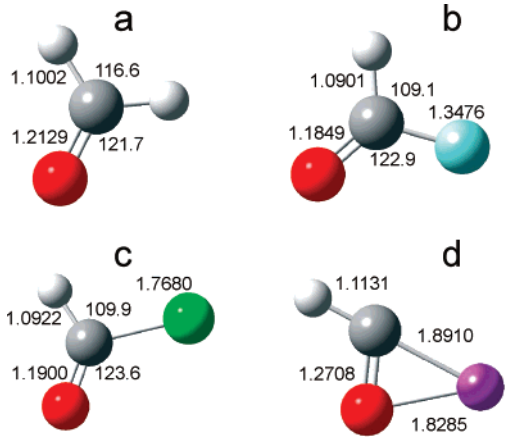

Figure 1. MP2/aug-cc-pVTZ optimized structures of the ground-state molecules HRCO (R = H, F, Cl, Li): (a) H_2CO; (b) HFCO; (c) HClCO; (d) HLiCO. Bond lengths are given in Å, and bond angles, in deg.

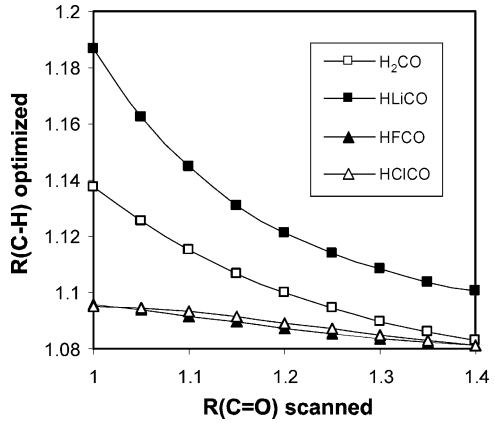

Figure 2. MP2/aug-cc-pVTZ optimized C−H distances as obtained from scans of the C═O distances of HRCO molecules (R = H, F, Cl, Li).

finding is in agreement with the early vibrational spectroscopic data on the complex of dimethyl ether with H_2O.[22] Some recent experimental[23a,b] and theoretical[23c,d] results also show that blue-shifted C−H frequencies may appear through mediation via remote intermolecular interactions.

The present work is aimed to put forward our previous study on the $H_2CO-(HF)_n$ complexes,[16a] primarily addressing the following issues: (a) a deeper understanding of the effects of cooperativity in cyclic hydrogen-bonded systems interacting with the guest molecule of the NIC type; (b) how the substitution in the guest molecule modifies the intramolecular coupling, changes the cooperative behavior, increases or reduces the magnitude of the blue shift, or even converts it to a red shift. The series of substituted formaldehydes HRCO with R = H, Li, F, and Cl is chosen as guest molecules, whereas HF and H_2O molecules, known to form cyclic clusters, are selected as hosts or interacting partners. The monomers HRCO, the dimers HRCO−HF and HRCO−H_2O, and the cyclic complexes HRCO−$(HF)_2$, HRCO−$(HF)_3$, HRCO−$(H_2O)_2$, and HRCO−$(H_2O)_3$ are studied in the present work, with particular emphasis on their structural and vibrational properties, and on the analysis of selected sections of the monomer and dimer potential energy surfaces (PES).

2. Computational Methodology

All calculations of the title complexes were performed within the second-order perturbation Møller−Plesset frozen-core method (MP2)[24] in conjunction with the extended Dunning-type basis set aug-cc-pVTZ,[25] using the GAUSSIAN 03 suite of programs.[26] Because of the floppy nature of the title complexes, all geometry optimizations were carried out with the option "TIGHT". Appropriate intra- and intermolecular scans of the monomer and dimer PESs were carried out at the same computational level. Harmonic vibrational frequencies were calculated to adequately characterize the minima. The calculated Cartesian force constants were transformed to internal force constants using the GAR2PED program.[27] Because the structural distortions and frequency shifts are the chief concern in the present work, the corrections of the stabilization energy ΔE by the zero-point energy (ZPE) and basis-set-superposition-error (BSSE) were dispensed with. We, however, report $\Delta E_a^{(n)}$, the stabilization energy with respect to the asymptotically separated ground-state HRCO and $(HF)_n$ or $(H_2O)_n$ cluster, and $\Delta E_b^{(n)}$, the stabilization energy with respect to HRCO and *n*HF or *n*H_2O molecules (note that $\Delta E_a^{(1)} = \Delta E_b^{(1)} := \Delta E^{(1)}$). The natural bond orbital (NBO) analysis was invoked to illustrate the intramolecular NIC feature of the isolated H_2CO molecule and its modifications caused by the interactions of H_2CO with $(HF)_n$ and $(H_2O)_n$ using the selected intermolecular scans.

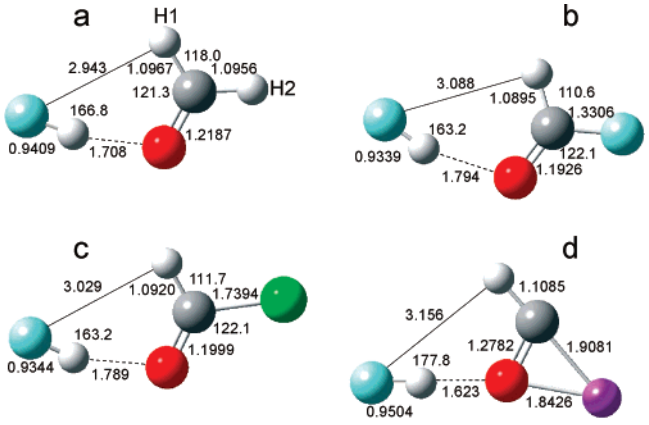

Figure 3. MP2/aug-cc-pVTZ optimized structures of the ground-state dimers HRCO−HF (R = H, F, Cl, Li): (a) H_2CO−HF; (b) HFCO−HF; (c) HClCO−HF; (d) HLiCO−HF. Bond lengths are given in Å, and bond angles, in deg.

TABLE 1: MP2/aug-cc-pVTZ Harmonic Stretching Frequencies, Infrared Intensities, and Force Constants of Substituted Formaldehydes HRCO (R = H, F, Cl, Li)[a]

R	H	F	Cl	Li
ν(C−H)	2973 (67) sym 3047 (88) asym	3158 (17)	3109 (14)	2839 (257)
ν(C═O)	1753 (68)	1847 (254)	1782 (316)	1467 (120)
ν(C−R)		1074 (270)	749 (226)	701[b] (132)
$k_{C-H,C-H}$	5.00	5.47	5.32	4.41
$k_{C=O,C=O}$	12.50	14.48	13.82	8.99
$k_{C=O,C-H}$	0.522	0.262	0.309	0.541

[a] Frequencies in cm^{-1}, infrared intensities in $km \cdot mol^{-1}$ in parentheses, and force constants in $mdyne \cdot Å^{-1}$. [b] Due to the ring structure of HLiCO (vide Figure 1), this mode is actually a combination of the Li−C and Li−O stretches.

3. Results and Discussion

3.1. HRCO Monomers. Many aspects of the effects of substitution of carbonyl compounds have already been discussed in the literature.[21,28] Our goal is to grip the quintessential trends of how the substitution affects the properties of the title complexes which are related to their structures, vibrational frequencies, and the intramolecular couplings between the C−H and C═O degrees of freedom.

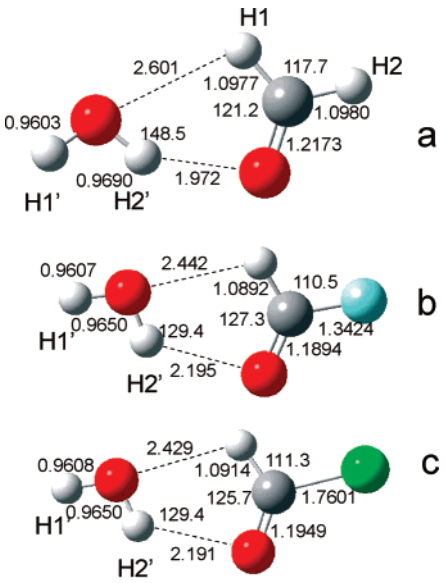

Figure 4. MP2/aug-cc-pVTZ optimized structures of the ground-state dimers HRCO−H_2O (R = H, F, Cl): (a) H_2CO−H_2O; (b) HFCO−H_2O; (c) HClCO−H_2O. Bond lengths are given in Å, and bond angles, in deg.

For this purpose, we begin with the HRCO monomers (R = H, Li, F, Cl) and display their optimized structures in Figure 1. The diagonal harmonic force constants $k_{C-H,C-H}$ and $k_{C=O,C=O}$, and the coupling force constant $k_{C=O,C-H}$ of these monomers are given in Table 1. Compared to the parent H_2CO molecule, the C−H and the C═O bonds are shorter in HFCO and HClCO, and considerably longer in HLiCO. This trend is mirrored in the vibrational frequencies and infrared intensities, and in the force constants as well. The C−H and the C═O stretching frequencies of HFCO and HClCO are blue-shifted relative to H_2CO, whereas their large red shifts occur in HLiCO. Correspondingly, the infrared intensities of the C−H stretching modes are lowered and those of the C═O stretchings are, on the contrary, increased.

What is of central importance for the ongoing discussion is the mode of response of a given guest molecule HRCO to an external perturbation, e.g., to a specific intermolecular interaction with the HF and H_2O clusters. As follows from the structure of the dimers that will be discussed in the next subsection, this response mode has its origin in the formation of hydrogen bonds to the C═O group, i.e., the conventional C═O···H−F and C═O···H−O hydrogen bonds that obviously influence the C═O bond length. The next questions to ask are how does the response mode spread over the entire HRCO molecule and, particularly, how do its C−H bonds respond to the perturbation of the C═O bond? The latter is answered in Figure 2, demonstrating that all four HRCO monomers respond negatively due to their NIC; that is, their R(C−H) contracts while R(C═O) stretches, albeit to a very different extent for different substituent R. This implies that the slope of the ratio ΔR(C−H)/ΔR(C═O), hereafter defined as the response factor α_R(H−C═O) := ΔR(C−H)/ΔR(C═O), is negative for ∀ R and much smaller, by the absolute value, for HFCO and HClCO compared to H_2CO and HLiCO.

By a direct analogy with the related work on formaldehyde[16a] and fluoromethanes,[19a] the response factor α_R(H−C═O) of HRCO can be explicitly expressed within the harmonic force-field approach, confined to the stretching degrees of freedom, in terms of the so-called harmonic response factor α_R^h(H−C═O) ≈ $-k_{C=O,C-H}/k_{C-H,C-H}$ (see eqs 4−6 of ref 16a for details).

TABLE 2: Selected MP2/aug-cc-pVTZ Properties of the Dimers HRCO−HF (R = H, F, Cl, Li)

R	H[a]	F	Cl	Li
ΔR(H−F) (mÅ)	18.2	12.2	12.7	28.7
ΔR(C−H) (mÅ)	**−3.5**	**−0.6**	**−0.2**	**−4.6**
ΔR(C−R) (mÅ)	−4.6	−17.0	−28.6	17.1
ΔR(C═O) (mÅ)	5.8	7.8	9.9	7.6
ν(H−F) (cm^{-1})[b]	3693 (946)	3852(698)	3839 (861)	3469 (1668)
$\Delta\nu$(H−F) (cm^{-1})[c]	−431 (7.8)	−272 (5.8)	−285 (7.1)	−755 (13.8)
ν(C−H) (cm^{-1})[b]	3017[d] (46) 3115[e] (39)	3172 (5)	3121 (3)	2906 (120)
$\Delta\nu$(C−H) (cm^{-1})	**44**,[d] **68**[e]	**14**	**12**	**67**
ν(C═O) (cm^{-1})[b]	1740 (71)	1820 (310)	1746 (369)	1455 (155)
$\Delta\nu$(C═O) (cm^{-1})	−13	−27	−36	−12
ν(C−R) (cm^{-1})		1135 (248)	812 (127)	679 (141)
$\Delta\nu$(C−R) (cm^{-1})		61	63	−22
$\Delta E^{(1)}$ (kcal·mol^{-1})	−8.57	−6.18	−6.08	−12.06

[a] Data from ref 13a. [b] Infrared intensity in km·mol^{-1} in parentheses. [c] Intensity enhancement relative to the HF monomer in parentheses. [d] Symmetric mode. [e] Asymmetric mode.

TABLE 3: Selected MP2/aug-cc-pVTZ Properties of the Dimers HRCO−H_2O (R = H, F, Cl)

R	H[a]	F	Cl
ΔR(O−H) (mÅ)	7.6, −1.1	3.6, −0.7	3.6, −0.6
ΔR(C−H) (mÅ)	**−2.5**	**−0.9**	**−0.8**
ΔR(C−R) (mÅ)	−2.2	−5.2	−7.9
ΔR(C═O) (mÅ)	4.4	4.6	4.9
ν(O−H)[a] (cm^{-1})	3916[b] (117) 3712[c] (214)	3929[b] (118) 3785[c] (42)	3927[b] (126) 3785[c] (44)
$\Delta\nu$(O−H) (cm^{-1})	−31,[b] −110[c]	−18,[b] −37[c]	−20,[b] −37[c]
ν(C−H)[a] (cm^{-1})	2999[b] (54) 3092[c] (48)	3178 (3)	3131 (1)
$\Delta\nu$(C−H) (cm^{-1})	**26**,[b] **45**[c]	**20**	**22**
ν(C═O)[a] (cm^{-1})	1741 (48)	1829 (229)	1764 (275)
$\Delta\nu$(C═O) (cm^{-1})	−12	−18	−18
ν(C−R) (cm^{-1})		1092 (303)	765 (247)
$\Delta\nu$(C−R) (cm^{-1})		18	16
$\Delta E^{(1)}$ (kcal·mol^{-1})	−5.58	−4.94	−4.86

[a] Infrared intensity in km·mol^{-1} in parentheses. [b] Symmetric mode. [c] Asymmetric mode.

If the latter is negative, there exists the NIC between the bonds C−H and C═O, and the larger $|\alpha^h|$ is, the larger is this NIC. Using Table 1, we obtain that α^h is equal to −0.05, −0.06, −0.1, and −0.12 for R = F, Cl, H, and Li, respectively, which is in good agreement with the numerical values ΔR(C−H)/ΔR(C═O) obtained from the scans of R(C═O) vs R(C−H) and yielding, correspondingly, −0.040, −0.044, −0.110, and −0.112. Therefore, HLiCO and H_2CO feature the distinctly larger $|\alpha|$ than HFCO and HClCO and that is why we may expect that the title complexes with HLiCO and H_2CO exhibit stronger blue shifts compared to the complexes with HFCO and HClCO—it is, however, obvious that the validity of this suggestion strongly depends on whether the condition i is obeyed. Because the latter does for the title dimers, let us proceed with the computational proof of this suggestion to the next Subsection.

3.2. Dimers HRCO−HF and HRCO−H_2O. The H_2CO−HF and H_2CO−H_2O dimers have already been extensively treated at different computational levels,[29,30] including the substitution effects,[21,31,32] although the blue shifts of the C−H stretching modes of these dimers have so far only be discussed for the cases R = H.[16a,30f]

The equilibrium structures of the dimers HRCO−HF (R = H, Li, F, Cl) and HRCO−H_2O (R = H, F, Cl) are shown in Figures 3 and 4 (the HLiCO−H_2O dimer is excluded from the studied series because it has an entirely different structure). The key intramolecular bond lengths and their changes upon dimer formation, the selected stretching vibrational frequencies and

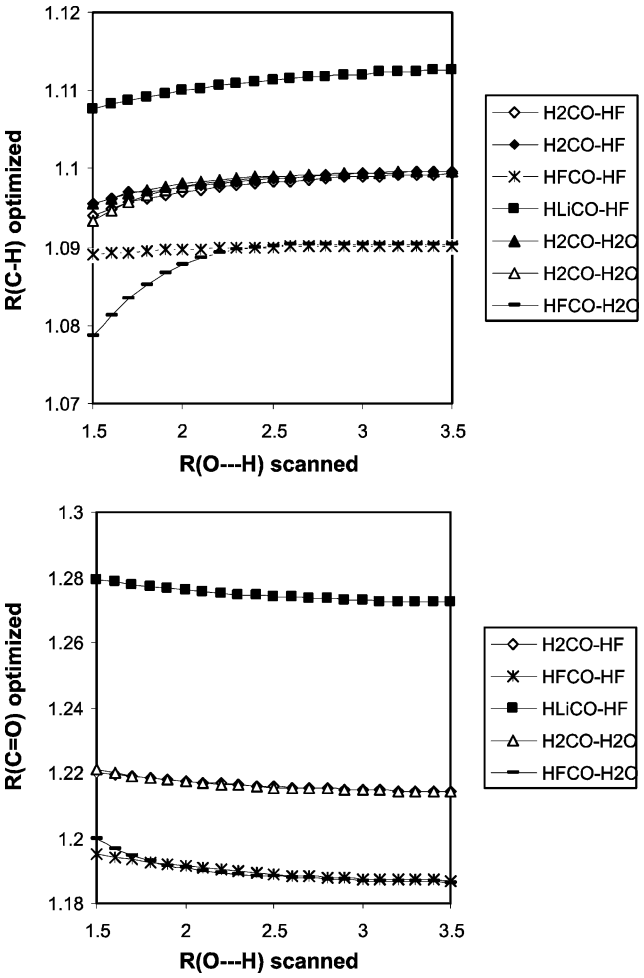

Figure 5. MP2/aug-cc-pVTZ optimized C−H and C═O distances as obtained from scans of the intermolecular O···H distances of HRCO−HF (R = H, F, Cl, Li) and HRCO−H_2O (R = H, F, Cl) dimers. The intermolecular (C═)O···H distance is chosen as the scan coordinate ranging from 1.5 to 3.5 Å. In these scans, the relative orientation of the two interacting partners is kept frozen by fixing the intermolecular C═O···H and O···H−F bond angles at the values of the corresponding minimum-energy dimer structures in the complexes with HF and the C═O···H and O···H−O bond angles in the complexes with H_2O. The rest of the internal coordinates are fully optimized. Due to the similarity between the complexes formed by HFCO and by HClCO, the scans for the latter are omitted.

concomitant infrared intensities, the frequency shifts taken with respect to the monomers, and the stabilization energies are collected in Tables 2 and 3. The latter satisfy the following inequalities for both HF and H_2O: $\Delta E^{(1)}$ (HClCO) > $\Delta E^{(1)}$(HFCO) > $\Delta E^{(1)}$(H_2CO) (>$\Delta E^{(1)}$(HLiCO) for HF only).

Let us first consider the series of HRCO−HF dimers. It is evident from the equilibrium structures of these dimers that they are held together by the F−H···O═C hydrogen bonds. Because of the orientation of the F−H molecule toward the C═O bond, the separation between the F atom and the H atom of HRCO is obviously too large to assume any hydrogen bonding interaction between them. A comparison of the interaction energies of these dimers and their intermolecular distances R(O···H(F)) implies that the strongest complex with $\Delta E^{(1)}$(HLiCO−HF) = −12.06 kcal·mol^{-1} is formed with HLiCO as the hydrogen bond acceptor, whereas the weakest complexes are formed with HFCO ($\Delta E^{(1)}$ = −6.18 kcal·mol^{-1}) and HClCO ($\Delta E^{(1)}$ = −6.08 kcal·mol^{-1}). Despite the absence of a direct hydrogen bond that involves the C−H bonds of the HRCO molecules, quite noticeable changes of R(C−H) upon dimer formation are,

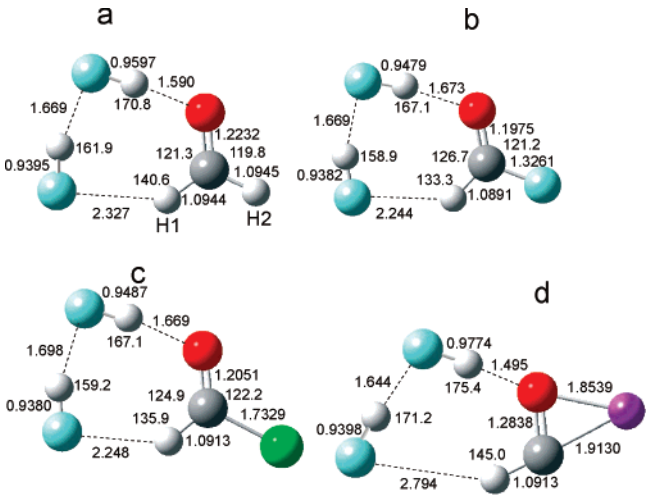

Figure 6. MP2/aug-cc-pVTZ optimized structures of the ground-state trimers HRCO−$(HF)_2$ (R = H, F, Cl, Li): (a) H_2CO−$(HF)_2$; (b) HFCO−$(HF)_2$; (c) HClCO−$(HF)_2$; (d) HLiCO−$(HF)_2$. Bond lengths are given in Å, and bond angles, in deg.

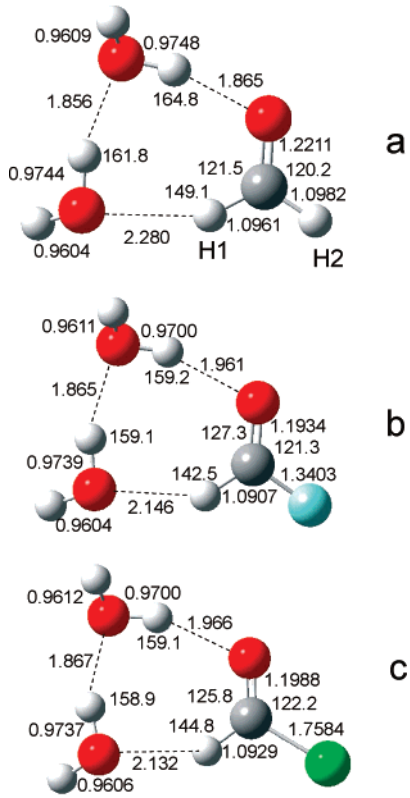

Figure 7. MP2/aug-cc-pVTZ optimized structures of the ground-state trimers HRCO−$(H_2O)_2$ (R = H, F, Cl): (a) H_2CO−$(H_2O)_2$; (b) HFCO−$(H_2O)_2$; (c) HClCO−$(H_2O)_2$. Bond lengths are given in Å, and bond angles, in deg.

however, observed. Evidently, they are caused by the intramolecular couplings that are mainly mediated by the distortion of the C═O bond under its interaction with HF. The shortening of the C−H bond is considerably larger in the complexes HLiCO−HF and H_2CO−HF compared to HFCO−HF and HClCO−HF. The calculated blue shift $\Delta\nu$(C−H) of HLiCO−HF amounts to 67 cm^{-1}, which is close to 56 cm^{-1}, the mean $\Delta\nu$(C−H) of the symmetric and asymmetric C−H stretches of H_2CO, whereas that of HFCO and HLiCO is much smaller, viz., 14 and 12 cm^{-1}, respectively. All four dimers are characterized by lower infrared intensities of the C−H stretching vibrations than in the monomers. The strongest shifts correspond to the

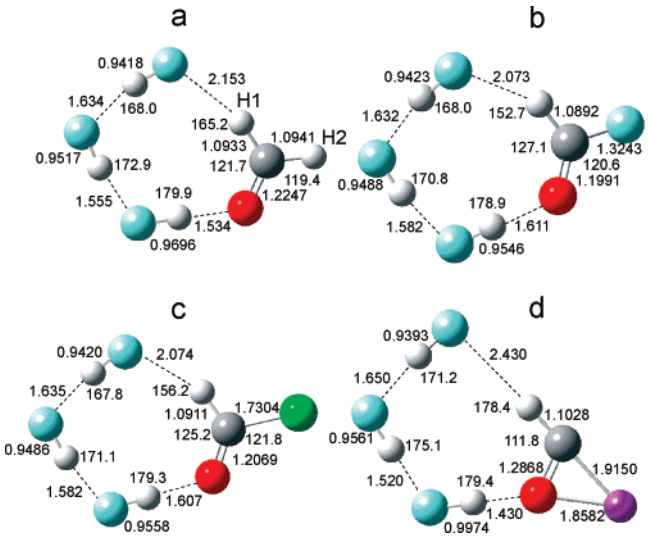

Figure 8. MP2/aug-cc-pVTZ optimized structures of the ground-state tetramers HRCO−(HF)$_3$ (R = H, F, Cl, Li): (a) $H_2CO-(HF)_3$; (b) HFCO−(HF)$_3$; (c) HClCO−(HF)$_3$; (d) HLiCO−(HF)$_3$. Bond lengths are given in Å, and bond angles, in deg.

red shifts of ν(H−F) in the conventional F−H··O═C hydrogen bonds which, together with their intensity enhancements, satisfy the canonical trends in the interaction strength.

The hydrogen bond to the C═O group casts also as the leading intermolecular contact in the complexes of HRCO (R = H, F, and Cl) with H_2O shown in Figure 4, although their hydrogen bond distances are significantly longer compared to the complexes with HF. However, unlike the HRCO−HF complexes, there appear secondary contacts O···H−C which, by many features, are at the border of weak hydrogen bonds. Therefore, in contrast to the HRCO−HF, the HRCO−H_2O dimers can be considered as cyclic complexes. Because H_2O is the weaker proton donor, the leading O−H···O═C hydrogen bonds of the HRCO−H_2O complexes are weaker and their interaction energies are considerably lower than of the HRCO−HF counterparts. As a consequence, the red shifts of ν(O−H) are smaller compared to $\Delta\nu$(H−F) in the HRCO−HF series. On the other hand, the range of the blue shifts of the C−H stretching mode is significantly narrower in the HRCO−H_2O series, and by analogy with the HRCO−HF series, $\Delta\nu$(C−H) is larger for H_2CO-H_2O than for HFCO−H_2O and HClCO−H_2O.

The fact that the contraction of the C−H bond in all dimers is largely a direct consequence of the response to the hydrogen bond formation at the carbonyl group can be illustrated by a series of intermolecular scans. The (C═)O···H distance was chosen as the scan coordinate ranging from 1.5 to 3.5 Å. In these scans, the relative orientation of the two interaction partners is kept frozen by fixing the intermolecular C═O···H and O···H−F bond angles at the values of the corresponding dimer minima in the complexes with HF, and the C═O···H and O···H−O bond angles in the complexes with H_2O. The remaining internal coordinates are fully optimized in these scans. Due to the similarity between the complexes formed with HFCO and those with HClCO, the scans for the latter are omitted. The optimized C═O and C−H distances resulting from these scans are shown in Figure 5 which allows us to conclude that (a) as anticipated, the formation of the hydrogen bonds F−H···O═C and O−H···O═C leads to elongation of the C═O bond and (b) this elongation of the C═O bond, in turn, causes the C−H bond(s) to contract.

This is precisely the pattern dictated by the negative intramolecular coupling between the C═O and C−H bonds demon-

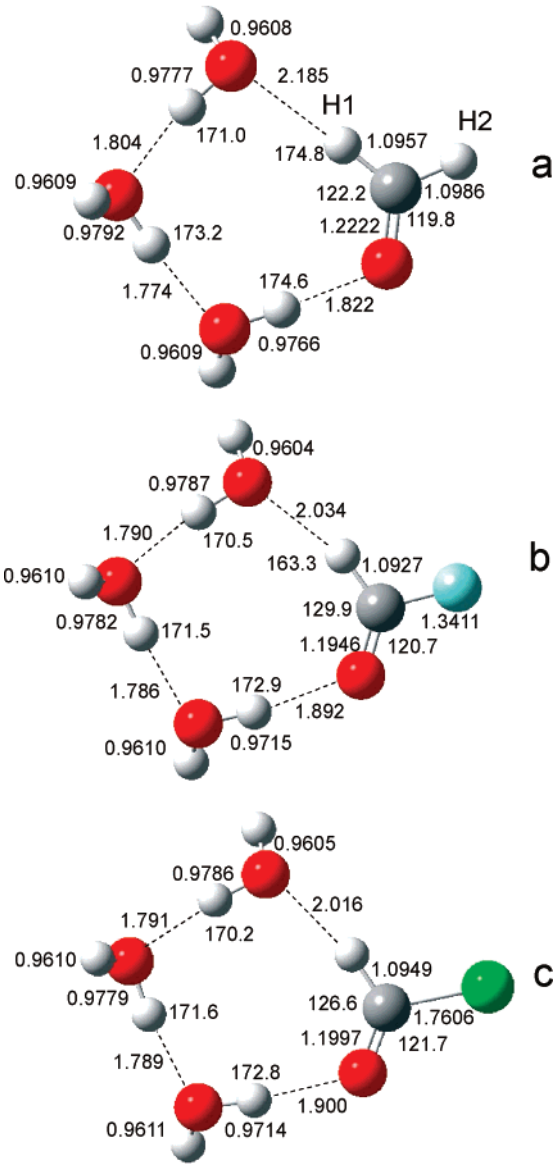

Figure 9. MP2/aug-cc-pVTZ optimized structures of the ground-state tetramers HRCO−(H$_2$O)$_3$ (R = H, F, Cl): (a) $H_2CO-(H_2O)_3$; (b) HFCO−(H$_2$O)$_3$; (c) HClCO−(H$_2$O)$_3$. Bond lengths are given in Å, and bond angles, in deg.

strated in Figure 2 for the isolated monomers. It is interesting to mention a rather strong contraction of the C−H bond of HFCO−H_2O that is caused by the presence of the short secondary contact C−H···O formed in this complex. When compressing the intermolecular (C═)O···H distance and keeping the relative orientation of the interacting molecules fixed, this secondary contact comes into the range of a strong C−H···O hydrogen bond. The formation of the C−H···O or C−H···F hydrogen bonds may also cause blue shifts. This effect will be considered for larger rings.

3.3. Cyclic Clusters HRCO−(HF)$_n$ and HRCO−(H$_2$O)$_n$, n = 2, 3. Among the title complexes, only $H_2CO-(HF)_n$[19a] and $H_2CO-(H_2O)_2$[30f] have been studied earlier. The equilibrium structures of the cyclic title trimers and tetramers are correspondingly shown in Figures 6 and 7 and in Figures 8 and 9. Their selected stretching vibrational frequencies, infrared intensities, the frequency shifts relative to the monomers, and the stabilization energies are presented in Tables 4−6.

Turning first to the series HRCO−$(HF)_2$ and HRCO−$(HF)_3$, we observe a progressive contraction of all intermolecular

TABLE 4: Selected MP2/aug-cc-pVTZ Properties of the Clusters HRCO−(HF)$_n$ (R = H, F, Cl, Li, and n = 2, 3)

R	H[a]	F	Cl	Li
n= 2				
ΔR(H−F) (mÅ)	16.8, 38.0	16.5, 26.2	16.3, 27.0	18.1, 55.7
ΔR(C−H) (mÅ)	**−5.8**	**−1.1**	**−0.9**	**−7.7**
ΔR(C−R) (mÅ)	−5.7	−21.5	−35.1	22.0
ΔR(C═O) (mÅ)	10.3	12.7	15.1	13.0
ν(H−F)[b] (cm^{-1})	3763 (645)	3799 (662)	3801 (661)	3745 (666)
	3325 (1397)	3571 (968)	3551 (1257)	2988 (1802)
$\Delta\nu$(H−F)[c] (cm^{-1})	−361 (5.3)	−325 (5.5)	−323 (5.5)	−379 (5.5)
	−799 (11.5)	−553 (8.0)	−573 (10.4)	−1136 (14.9)
ν(C−H)[b] (cm^{-1})	3036[d] (77)	3187 (9)	3140 (13)	2935 (740)
	3149[e] (12)			
$\Delta\nu$(C−H) (cm^{-1})	**63**,[d] **102**[e]	**29**	**31**	**96**
ν(C═O)[b] (cm^{-1})	1728 (72)	1798 (324)	1725 (389)	1439 (165)
$\Delta\nu$(C═O) (cm^{-1})	−13	−27	−36	−12
ν(C−R)[b] (cm^{-1})		1152 (230)	792 (403)	673 (145)
$\Delta\nu$(C−R) (cm^{-1})		61	43	22
$\Delta E^{(2)}$ (kcal·mol^{-1})	−13.75[f] (−18.46)[g]	−11.33 (−16.04)	−11.04 (−15.75)	−17.24 (−21.95)
n = 3				
ΔR(H−F) (mÅ)	20.1, 30.0, 47.9	20.6, 27.1, 32.9	20.3, 26.9, 34.1	17.8, 34.4, 75.7
ΔR(C−H) (mÅ)	−6.9	−0.9	−1.1	−10.3
ΔR(C−R) (mÅ)	−6.1	−23.4	−37.6	24.0
ΔR(C═O) (mÅ)	11.8	14.3	16.9	16.8
ν(H−F)[b] (cm^{-1})	3726 (742)	3724 (708)	3729 (747)	3763 (686)
	3526 (1041)	3595 (1161)	3593 (1142)	3435 (1141)
	3118 (1784)	3406 (1416)	3381 (1861)	2607 (3266)
$\Delta\nu$(H−F)[c] (cm^{-1})	−398 (6.1)	−400 (5.9)	−395 (6.2)	−361 (5.7)
	−598 (8.6)	−529 (9.6)	−531 (9.4)	−689 (9.4)
	−1006 (14.7)	−718 (11.7)	−763 (15.4)	−1517 (27.0)
ν(C−H)[b] (cm^{-1})	3040[d] (317)	3188 (31)	3145 (50)	2997 (30)
	3165[e] (19)			
$\Delta\nu$(C−H) (cm^{-1})	**67**,[d] **118**[e]	30	36	158
ν(C═O)[b] (cm^{-1})	1728 (93)	1791 (378)	1718 (453)	1431 (205)
$\Delta\nu$(C═O) (cm^{-1})	−25	−49	−64	−36
ν(C−R)[b] (cm^{-1})		1152	795 (248)	673 (136)
$\Delta\nu$(C−R) (cm^{-1})		78	46	−28
$\Delta E^{(3)}$ (kcal·mol^{-1})	−12.95[f] (−28.41)[g]	−10.95 (−26.06)	−10.20 (−25.66)	−16.30 (−31.76)

[a] Data from ref 13a. [b] Infrared intensity in km·mol^{-1} in parentheses. [c] Intensity enhancement relative to the HF monomer. [d] Symmetric mode. [e] Asymmetric mode. [f] $\Delta E_a^{(n)}$ defined as $\Delta E_a^{(n)} = E$[HRCO−(HF)$_n$] − E[HRCO] − E[(HF)$_n$]. [g] $\Delta E_b^{(n)}$ defined as $\Delta E_b^{(n)} = E$[HRCO−(HF)$_n$] − E[HRCO] − nE[HF] in parentheses.

TABLE 5: Selected MP2/aug-cc-pVTZ Properties of the Clusters HRCO−(H$_2$O)$_2$ (R = H, F, Cl)

R	H[a]	F	Cl
n = 2			
ΔR(O−H)[a] (mÅ)	13.4, 13.0	8.6, 12.5	8.6, 12.3
ΔR(O−H)[b] (mÅ)	−0.5, −1.0	−0.3, −1.0	−0.2, −0.8
ΔR(C−H) (mÅ)	**−4.1**	**0.6**	**0.7**
ΔR(C−R) (mÅ)	−2.0	−7.3	−9.7
ΔR(C═O) (mÅ)	8.2	8.6	8.8
ν(O−H)[a,c] (cm^{-1})	3636 (526)	3710 (318)	3709 (101)
	3590 (359)	3621 (346)	3624 (321)
ν(O−H)[b,c] (cm^{-1})	3907 (88)	3908 (100)	3907 (101)
	3901 (116)	3906 (142)	3904 (162)
$\Delta\nu$(O−H)[a] (cm^{-1})	−186, −232	−112, −199	−113, −198
$\Delta\nu$(O−H)[b] (cm^{-1})	−40, −46	−39, −41	−40, −43
ν(C−H)[c] (cm^{-1})	3000[d] (85)	3161 (25)	3116 (51)
	3113[e] (9)		
$\Delta\nu$(C−H) (cm^{-1})	**27**,[d] **66**[e]	3	7
ν(C═O)[c] (cm^{-1})	1731 (59)	1808 (271)	1744 (323)
$\Delta\nu$(C═O) (cm^{-1})	−22	−39	−38
ν(C−R)[c] (cm^{-1})		1095 (325)	770 (195)
$\Delta\nu$(C−R) (cm^{-1})		21	21
$\Delta E^{(2)}$ (kcal·mol^{-1})	−9.20[f] (−14.38)[g]	−9.23 (−14.41)	−8.99 (−14.17)

[a] OH in hydrogen bond. [b] Free OH. [c] Infrared intensity in km·mol^{-1} in parentheses. [d] Symmetric mode. [e] Asymmetric mode. [f] $\Delta E_a^{(2)}$ defined as $\Delta E_a^{(2)} = E$[HRCO−(H$_2$O)$_2$] − E[HRCO] − E[(H$_2$O)$_2$]. [g] $\Delta E_b^{(2)}$ defined as $\Delta E_b^{(2)} = E$[HRCO−(H$_2$O)$_2$] − E[HRCO] − 2E[H$_2$O] in parentheses.

distances, R((C═)O···H(−F)) < R((F−)H···F(−H)) ≪ R((C−)H···F(−H)), as the ring size increases - the shortest R((C═)O···H(−F)) and longest R((C-)H···F(−H)) are predicted for the complexes HLiCO−(HF)$_{2\le n\le 3}$. In particular, the C−H···F contact is indeed sufficiently short for all R to be treated as a hydrogen bond.

The involved C−H bond is also shortened with respect to the monomers, much stronger in H$_2$CO and HLiCO than in HFCO and HClCO where it remains almost unchanged, within −0.0001 to −0.002 Å, through the entire series of the complexes HFCO−(HF)$_{1\le n\le 3}$ and HClCO−(HF)$_{1\le n\le 3}$. As a result, the blue shifts $\Delta\nu$(C−H) are largest in the HLiCO−(HF)$_{1\le n\le 3}$ and H$_2$CO−(HF)$_{1\le n\le 3}$ clusters, reaching +158 cm^{-1} for HLiCO−(HF)$_3$. It is worth mentioning in this regard that the H−F stretching modes of the cyclic (HF)$_n$ complexes undergo quite substantial red shifts characterized by significantly increased infrared intensities.[33]

The structures of the HRCO−(H$_2$O)$_{2\le n\le 3}$ clusters differ from those of HRCO−(HF)$_{2\le n\le 3}$ in several aspects (cf. Figures 7 and 9 and see also the early work[30f] on the H$_2$CO−(H$_2$O)$_2$ complex). First, the intermolecular C═O···H−O hydrogen bonds are distinctly longer, by ∼0.3 Å, than their counterparts in HRCO−(HF)$_n$. Second, depending on the substituent R, the C−H···O−H hydrogen bonding reveals a rather complicated pattern compared to the C−H···F−H hydrogen bonds: for R = H, the C−H···O−H hydrogen bond contracts by 0.06 Å for n =2 and elongates by 0.03 Å for n = 3, whereas for R = F and Cl, it contracts by 0.1 Å for n = 2 and by 0.4−0.6 Å for n = 3. In the complexes HFCO−(H$_2$O)$_3$ and HClCO−(H$_2$O)$_3$, the C−H bond approaches the neighboring water molecule at 2.034 and 2.016 Å, respectively. These differences in the

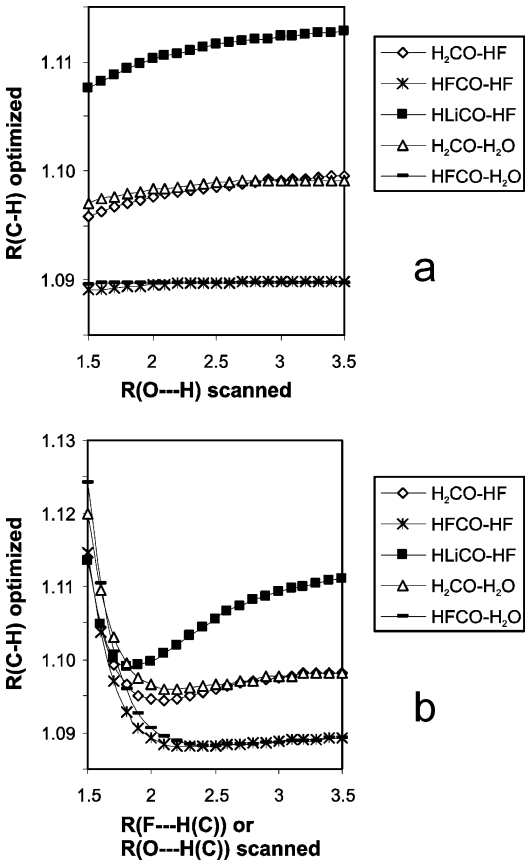

Figure 10. MP2/aug-cc-pVTZ optimized C−H distances as obtained from scans of the intermolecular (a) O···H distances of HRCO−$(HF)_2$ and HRCO−$(OH_2)_2$ trimers (R = H, F, Cl, Li) and (b) (C)H···O and (C)H···F distances of HRCO−$(HF)_2$ and HRCO−$(OH_2)_2$ trimers (R = H, F, Cl, Li).

TABLE 6: Selected MP2/aug-cc-pVTZ Properties of the Clusters HRCO−$(H_2O)_3$ (R = H, F, and Cl)

R	H[a]	F	Cl
$n = 2$			
ΔR(O−H)[a] (mÅ)	16.3, 17.8, 15.2	17.3, 16.8, 10.1	17.2, 16.5, 10.0
ΔR(O−H)[b] (mÅ)	−0.6, −0.5, −0.5	−1.0, −0.4, −0.4	−0.9, −0.4, −0.3
ΔR(C−H) (mÅ)	**−4.5**	**2.6**	**2.7**
ΔR(C−R) (mÅ)	−1.6	−6.5	−7.4
ΔR(C═O) (mÅ)	9.3	9.8	9.7
ν(O−H)[a,c] (cm^{-1})	3587 (370)	3682 (436)	3681 (523)
	3567 (927)	3567 (625)	3570 (663)
	3499 (610)	3508 (645)	3510 (603)
ν(O−H)[b] (cm^{-1})	3904 (83)	3904 (100)	3903 (114)
	3900 (109)	3903 (134)	3902 (140)
	3898 (96)	3898 (96)	3897 (98)
$\Delta\nu$(O−H)[a] (cm^{-1})	−235, −255, −323	−140, −255, −314	−141, −252, −312
$\Delta\nu$(O−H)[b] (cm^{-1})	−43, −47, −49	−43, −44, −49	−44, −45, −50
ν(C−H)[c] (cm^{-1})	2996[d] (93)	3132 (77)	3086 (139)
	3119[e] (11)		
$\Delta\nu$(C−H) (cm^{-1})	**23**,[d] **72**[e]	**−26**	**−23**
ν(C═O)[b,c] (cm^{-1})	1734 (77)	1801 (319)	1739 (381)
$\Delta\nu$(C═O) (cm^{-1})	−19	−46	−43
ν(C−R)[c] (cm^{-1})		1090 (321)	754 (246)
$\Delta\nu$(C−R) (cm^{-1})		16	6
$\Delta E^{(3)}$ (kcal·mol^{-1})	−7.02[f] (−23.31)[g]	−7.48 (−23.77)	−7.21 (−23.50)

[a] OH in hydrogen bond. [b] Free OH. [c] Infrared intensity in km·mol^{-1} in parentheses. [d] Symmetric mode. [e] Asymmetric mode. [f] $\Delta E_a^{(3)}$ defined as $\Delta E_a^{(3)} = E$[HRCO−$(H_2O)_3$] − E[HRCO] − E[$(H_2O)_3$]. [g] $\Delta E_b^{(3)}$ defined as $\Delta E_b^{(3)} = E$[HRCO−$(H_2O)_3$] − E[HRCO] − $3E$[H_2O] in parentheses.

bonding patterns can easily be explained in terms of the stronger hydrogen bond donor and weaker hydrogen bond acceptor characteristics of the hydrogen fluoride molecule as compared to the water molecule.

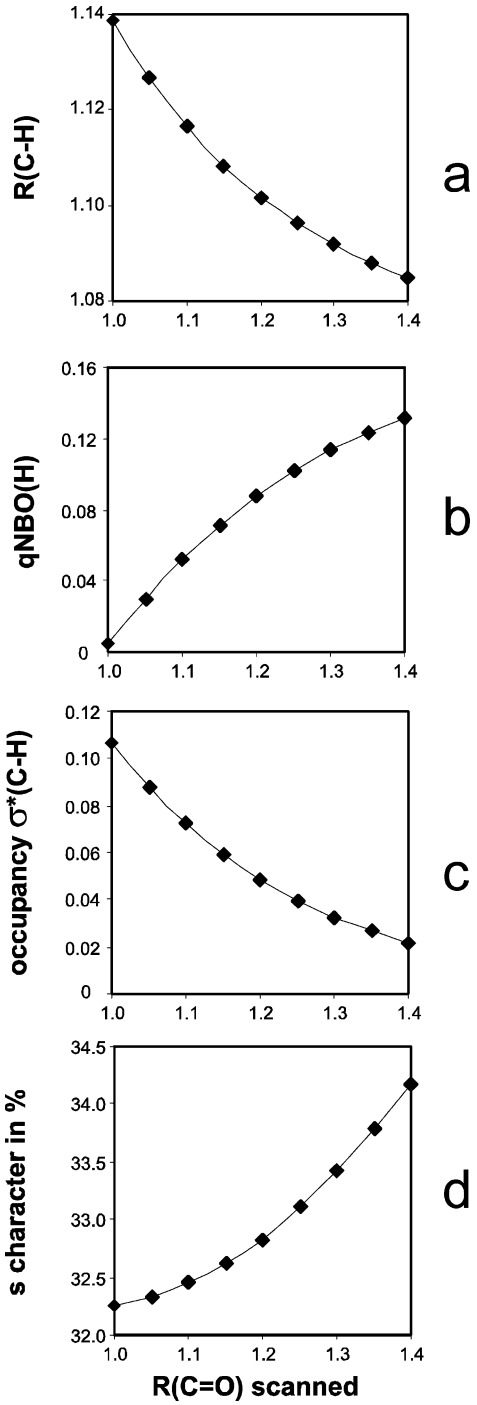

Figure 11. NBO analysis of the H_2CO monomer along the scan coordinate R(C═O). (a) R(C−H); (b) the NBO charge q_{NBO}(H) on the hydrogen of the C−H bond; (c) the occupancy of the σ^*(A−H) antibonding MO; (d) the %s-character of the hybrid MO.

The C−H bonds of HRCO−$(H_2O)_{2\le n\le 3}$ behave differently from those of HRCO−$(HF)_{2\le n\le 3}$. In H_2CO−$(H_2O)_{2\le n\le 3}$, they contract by ca. −0.001 to −0.002 Å, yielding the concomitant small blue shifts of the ν(C−H)'s. In HFCO−$(H_2O)_{2\le n\le 3}$ and HClCO−$(H_2O)_{2\le n\le 3}$, they undergo elongations of ∼0.0015 Å ($n = 2$) and ∼0.0035 Å ($n = 3$) relative to HFCO and HClCO, respectively. The C−H stretching frequencies of the latter clusters are still slightly blue-shifted for $n = 2$, but converted to red-shifted ones for $n = 3$. We suggest that such a blue−red size-dependent transition occurs due to a considerable strength-

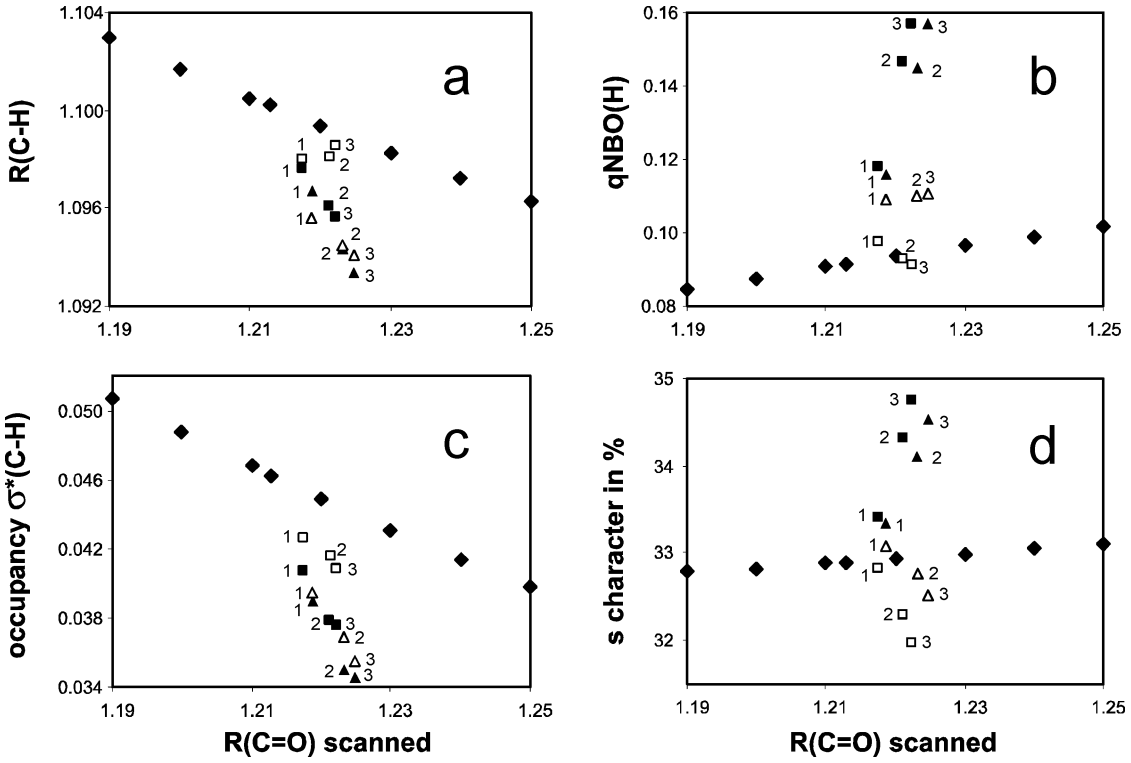

Figure 12. NBO analysis of the H_2CO monomer along the scan coordinate R(C═O) and of the $H_2CO-(HF)_n$ and $H_2CO-(H_2O)_n$ complexes at their optimized geometries: (a) R(C−H); (b) the NBO charge q_{NBO}(H) on the hydrogen of the C−H bond; (c) the occupancy of the σ^*(A−H) antibonding MO; (d) the %s-character of the hybrid MO. Definition of symbols: diamonds for the H_2CO monomer; triangles for $H_2CO-(HF)_n$; squares for $H_2CO-(H_2O)_n$; filled symbols for H1; and open symbols for H2. The adjacent numbers indicate n.

ening of the hydrogen bonding interaction between the C−H bond and the neighboring water molecule as proton acceptor that becomes competitive with the NIC acting from the remote water molecule through the C═O···H−O hydrogen bond.

To rationalize this suggestion, let us invoke the scan plots shown in Figure 10. These scan plots display the optimized C−H bond lengths resulting from selected scans of HRCO−HF and HRCO−H_2O dimers clipped from the corresponding trimers HRCO−$(HF)_2$ and HRCO−$(H_2O)_2$ with frozen relative orientations. Figure 10a that plots the scans of R(O···H) of the dimer in which the C═O bond acts as hydrogen bond acceptor is quite similar to Figure 5a. The difference between them is attributed to different relative orientations of the monomers. Recall that the latter figure qualitatively displays the NIC effect: a contraction of the hydrogen bond formed between HF or H_2O and the C═O bond causes the latter to elongate and in turn the vicinal C−H bond to contract. Figure 10b plots the scans of another type of these dimers in which the C−H bond of HRCO acts as the hydrogen bond donor either to HF or H_2O molecules. These are the structures usually associated with the term *blue-shifting hydrogen bonds*.

The first important result from these scans is that the C−H bond undergoes contraction for asymptotically large intermolecular F···H(−C) or O···H(−C) distances. The effect of the NIC of the HRCO molecules, which can be treated as underlying a possible blue-shifting mechanism is visible already for small perturbations of the monomers. At very short intermolecular F···H(−C) or O···H(−C) distances, however, the C−H bond elongates again. Thus, there must exist a turning point at which the blue shift is converted to a red shift. It is clearly quite sensitive to the donor (guest) molecule HRCO and to the hydrogen bond acceptor and appears at very short intermolecular distances for R = Li, whereas for R = H and R = F, it occurs, correspondingly, at about 1.8 Å and slightly larger at 2.0 Å. It is also worth mentioning that a stronger character of the hydrogen bond acceptor, such as H_2O in comparison to HF, is also evidenced from Figure 10b because the stronger the acceptor, the lower the tendency to blue shift. This behavior has already been discussed[19a] for the blue-shifted complex F_3CH-OH_2 with the weaker acceptor H_2O and the red-shifted one F_3CH-NH_3 with the stronger acceptor NH_3.

Apart from the effects of cooperativity that contribute to the equilibrium structures, vibrational spectra, and frequency shifts of the trimeric and tetrameric complexes, the nonadditivity effects are also manifested in the stabilization energies. $\Delta E_a^{(n)}$, defined as the stabilization energy of $H_2CO-(HF)_n$ with respect to H_2CO separated asymptotically from the optimal $(HF)_n$ cluster (i.e., the open dimer for $n = 2$ and the cyclic trimer for $n = 3$), and $\Delta E_b^{(n)}$, defined as the stabilization energy with respect to H_2CO and n separated HF molecules, are known at the MP2/aug-cc-pVTZ computational level for $n = 1 - 4$, together with the corresponding BSSE corrected values.[16a]

As seen in Tables 4−6, the trends in $\Delta E_a^{(n)}$ and $\Delta E_b^{(n)}$ are rather similar for all HRCO−$(HF)_n$ and HRCO−$(H_2O)_n$ clusters. $\Delta E_b^{(n)}$ increases with n, significantly beyond the assumption of additivity.[34] $\Delta E_a^{(n)}$ takes the maximum value at $n = 2$. The simple explanation of this behavior is that, upon formation of the cyclic trimer, two new hydrogen bonds, a strong C═O···H and a weak C−H···F or C−H···O, are formed. These two replace one sterically unfavorable hydrogen bond upon the formation of the cyclic tetramer, when HRCO is inserted into the preformed cyclic trimer, $(HF)_3$ or $(H_2O)_3$. At the same time, the steric strain of the other hydrogen bonds is partly released when the ring size increases from trimer to tetramer. As known from $H_2CO-(HF)_4$[16a] and from the series of pure cyclic $(HF)_n$ clusters,[33,35] and related systems,[33] $\Delta E_a^{(n)}$ is expected to further decrease with increasing ring size. Finally, it is worth noting that the effects of cooperativity in model sequential hydrogen-

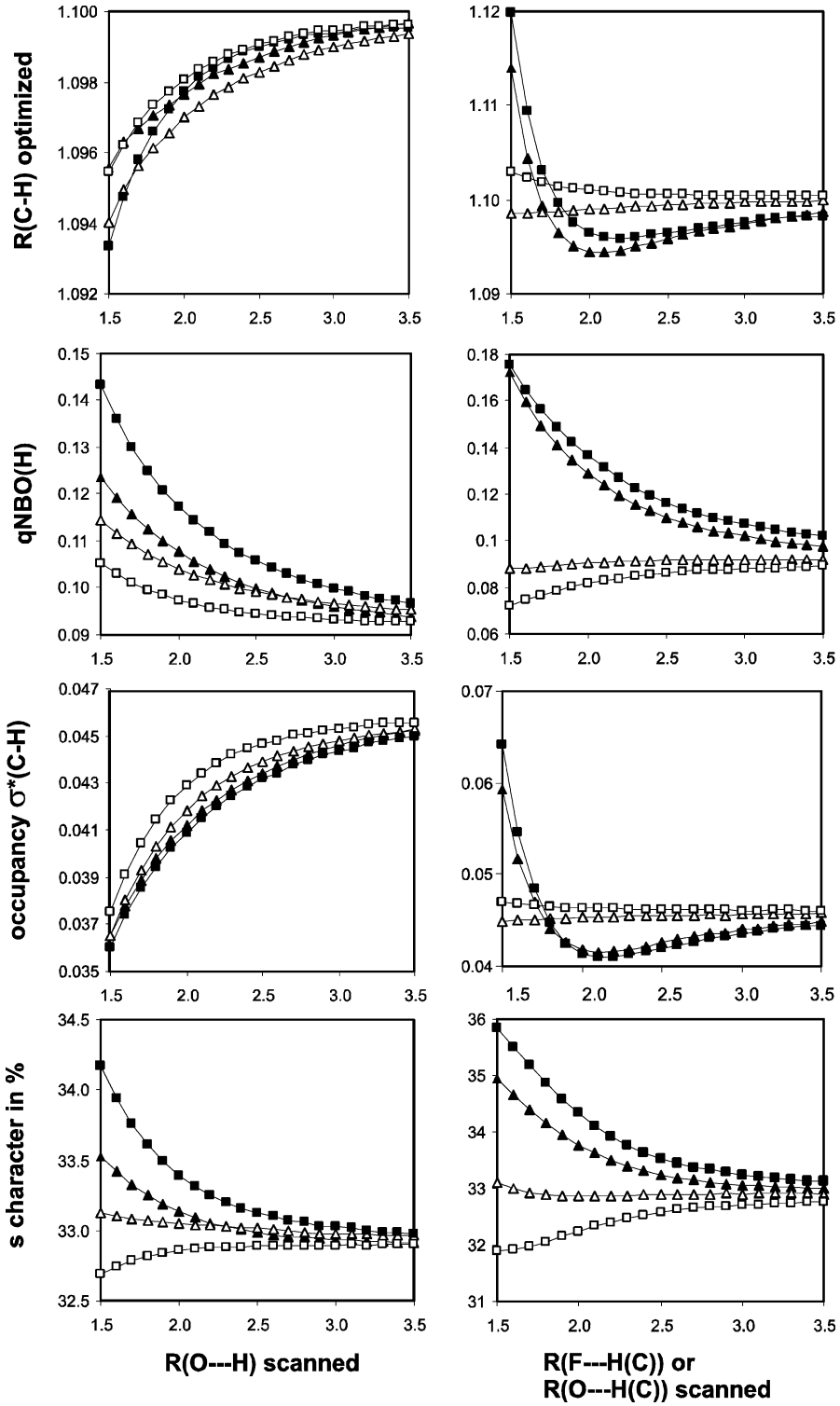

Figure 13. NBO analysis along intermolecular scans of the selected H_2CO-HF and H_2CO-H_2O dimers. Left column: H_2CO-HF and H_2CO-H_2O with C═O−H hydrogen bonds and relative orientation as in the optimized dimers (see Figure 5 for comparison). Right column: H_2CO-HF and H_2CO-H_2O dimers with C−H···F and C−H···O hydrogen bonds cut out from the cyclic trimer (see Figure 10b for comparison). Definition of symbols: triangles for H_2CO-HF; squares for H_2CO-H_2O; filled symbols for H1; and open symbols for H2.

bonded polymers $(H_2CO)_n$ and $(HFCO)_n$[36] are significantly weaker than in chain-like $(H_2O)_n$[37,38] or $(HF)_n$ polymers,[33,35] comparable with $(HCN)_n$.[33,35,39]

3.4. NBO Picture of NIC. The molecular orbital (MO) picture of the formation of the conventional X−H···Y hydrogen bonding interaction is typical:[40] an increase in the population or electron density of the σ^*(X−H) antibonding MO weakens the X−H bond and determines its elongation and concomitant red shift of ν(X−H); the cause is the intermolecular hyperconjugative n(Y) → σ^*(X−H) interaction that dominates for conventional, red-shifted hydrogen bonds. In contrast, the leading factor that governs the formation of nonconventional, blue-shifted hydrogen bonds is the rehybridization.[10] Within this context,[10] the interplay between the hyperconjugative and rehybridization mechanisms acting clearly in the opposite directions (see also the recent studies[41] quantifying this trend), and thus determining whether a given hydrogen bond is red- or blue-shifted, is a direct consequence of Bent's rule. Recall that

the rule states that the atom tends to maximize the amount of s-character in the hybrid MO with the larger amount of p-character toward more electronegative substituents. This results in a decrease of the effective electronegativity of the hydrogen atom within the X−H bond and in an increase of the s-character of the X hybrid MO that in turn increases the polarization of the X−H bond.

Figure 11 gives the MO picture of the intramolecular NIC of the isolated H_2CO molecule, which is also evidenced from its PES: When R(C═O) increases, (a) NIC contracts the C−H bonds and thus strengthens them (see also Figure 2); (b) NIC increases the NBO positive charges, q_{NBO}(H), on the hydrogen atoms and, as a consequence, the C−H bond polarization; (c) simultaneously with re-polarization of the C−H bonds, there occurs a decrease of the electron densities of the two C−H antibonding σ^*(C−H) MOs that, in contrast to the conventional hydrogen bonds, unambiguously implies strengthening and shortening of the C−H bonds and their C−H stretches are incurred to blue shifts; and (d) an increase in the s-character (rehybridization) of the σ^*(C−H) MOs occurs that strengthens the C−H bonds and causes their contraction. Notice that the importance of considering the intramolecular hyperconjugation separately has been advocated quite recently.[42]

As a matter of fact, the MO picture given in Figure 11 is valid only for the isolated H_2CO molecule. Its interaction with the $(H_2O)_n$ or $(HF)_n$ clusters drastically changes this picture. This is illustrated in Figure 12, which displays the plots similar to those in Figure 11 at a narrower scale and includes for comparison the analogous properties calculated for all $H_2CO-(HF)_n$ and $H_2CO-(H_2O)_n$ complexes. In Figure 12, we observe quite interesting trends with increasing cluster size. As discussed above, the bond length R(C═O) increases with increasing n. This is accompanied, as demonstrated in Figure 12a, by a stronger decrease of R(C−H) in $H_2CO-(HF)_n$ compared to that in $H_2CO-(H_2O)_n$. Moreover, as n increases, we also observe a strong increase of q_{NBO}(H) of H1 (Figure 12b), a decrease of the electron densities of the two C−H antibonding σ^*(C−H) MOs (Figure 12c), and some growth of the s-character of the C−H1 bonds which participates in the C−H···F or C−H···O hydrogen bonds. Evidently, the s-character of the C−H2 bond may even fall below that of the H_2CO monomer. Summarizing, the observed trends reveal the same direction as the C═O bond of the isolated monomer under stretching. Due to the intermolecular interactions and strong effects of cooperativity, the changes that occur in the cyclic complexes are significantly stronger.

Quite remarkable trends (see Figure 13) are unveiled by the NBO analysis of the intermolecular scans reported earlier in Figures 5 and 10b, which correspond to the approach of the monomers with fixed orientation as in the optimized dimers H_2CO-HF and H_2CO-H_2O with C═O···H (left column in Figure 13), and for the dimers clipped from the optimized trimers with C−H···F and C−H···O hydrogen bonds (right column). Let us first discuss the former case of the C═O···H approach, i.e., the formation of the conventional hydrogen bond that results in an increase of R(C═O) and that does not involve the H1 and H2 of the H_2CO molecule. A decrease of the intermolecular distance causes the C−H bonds to contract and thus increases the corresponding NBO charges q_{NBO}(H) and the s-character of these C−H bonds and, on the contrary, lowers the occupation of the σ^*(C−H) MOs. This picture precisely reflects the one found for the C═O bond of the isolated H_2CO monomer under stretching.

The right column of Figure 13 corresponds to the case when the C−H···F or C−H···O hydrogen bond is formed. Under contraction of the intermolecular distance, R(C−H1) shows the behavior already displayed in Figure 10b, whereas R(C−H2) is barely modified. With decreasing intermolecular distance, q_{NBO}(H1) and the s-character of the C−H1 bond both increase, whereas the corresponding C−H2 properties are not appreciably modifed. The occupation of the antibonding σ^*(C−H1) MO initially decreases and then increases, reaching the minimum in the vicinity of the optimized intermolecular distance corresponding to the cyclic trimer.

4. Summary and Conclusions

Let us recall that, about 7 years ago,[1−3,7−9] a few novel "hydrogen bonds" that revealed small blue shifts of only 10−20 cm^{-1} were considered in the context of the conventional hydrogen bonding theory as the exceptional phenomenon. It was a belief at that time that these blue-shifting hydrogen bonds are extremely weak and that their blue shifts fall within the range 10−40 cm^{-1} at most.

In the present work, we have performed model calculations on a series of dimers and cyclic clusters composed of HRCO as the guest molecule inserted into the $(HF)_n$ or $(H_2O)_n$ cyclic host clusters. We have demonstrated that, although the complexes are structurally very similar, they spread over from the blue- to red-shifted complexes, exhibiting, on the one side ($HLiCO-(HF)_3$), a quite noticeable blue shift $\Delta\nu$(C−H) of about 160 cm^{-1}, and on the other ($HFCO-(H_2O)_3$ and $HClCO-(H_2O)_3$), a small red shift. The magnitude of the blue shift depends on both the substituent R of the guest and the hydrogen bond donor and acceptor characteristics of the host molecules. The working key concept that allows us to predict whether a given molecule is in principle prone to shift its X−H (mostly C−H) stretching mode toward higher wavenumbers upon complex formation is the *negative intramolecular coupling* (NIC) that governs the contraction of the X−H bond under condition i. This NIC exists in the isolated monomer and can therefore be probed from the monomer PES. In the case of the HRCO molecules interacting with HF or H_2O, it is fairly obvious that the relevant coordinate, which is coupled to the C−H bond, is the C═O. If the latter is scanned for all four HRCO molecules, we have clearly demonstrated that, first, all of them display the NIC feature and, second, the strength of this coupling strongly depends on the substituent. The blue shifts of the C−H stretching vibrations calculated for all dimers faithfully follow the trends, largely predicted by the NIC and slightly perturbed by the different hydrogen bond donor strengths of HF and H_2O, and are therefore *not directly caused* by the formation of "blue-shifted" hydrogen bonds, because the latter are either absent as in HRCO−HF or too weak as in $HRCO-H_2O$. The leading role in their blue shifts is determined by the conventional hydrogen bonds of HF or H_2O to the C═O bond of the HRCO molecules. The blue shifts thus appear *indirectly*, via the coupling of C═O and C−H bonds, as a consequence of the NIC.

In the cyclic trimers and tetramers, the C−H bonds take part in the hydrogen bond formation and are therefore additionally influenced by the hydrogen bond acceptor. With the aid of appropriate intermolecular scans carried out for frozen relative orientation of the interacting molecules (Figures 5 and 10), we clearly observe that stronger hydrogen bonds to C═O tend to increase the blue shift via the *indirect* mechanism. However, whether the *direct* formation of the C−H···X hydrogen bonds leads to increasing or lowering of the blue shift depends on the strength of the NIC and on the hydrogen bond acceptor strength of the molecule with which the C−H···X hydrogen bond is

formed: a stronger acceptor strength tends to suppress a blue shift. This is illustrated by the concrete complexes of $HFCO-(H_2O)_3$ and $HClCO-(H_2O)_3$ where the interplay of a stronger hydrogen bond acceptor with a weaker NIC yields a small red shift, whereas for $HLiCO-(HF)_3$, the combination of a weaker acceptor strength and a larger $|\alpha|$, results in a noticeable blue shift.

The NBO analysis performed on the H_2CO monomer, on the optimized cluster structures, and for selected intermolecular scans has firmly demonstrated that the trends, visible already for the intramolecular scans of the isolated H_2CO monomer, are reencountered in the clusters, evidently modified by the hydrogen bond donor and acceptor strengths of HF and H_2O, and by the nonadditive behavior of the intermolecular interactions between the studied polar molecules.

Acknowledgment. E.S.K. gratefully thanks Profs. Camille Sandorfy and Austin Barnes for encouraging discussions and useful suggestions, and Francoise Remacle for warm hospitality. This work (E.S.K.) was partially supported by the EC FET-OPEN STREP Project MOLDYNLOGIC. The calculations were performed on the Linux-cluster Schrödinger III at the University of Vienna. We are grateful for ample supply of computer time at this installation. Finally, we are indeed thankful the reviewers for valuable comments and suggestions.

References and Notes

(1) Hobza, P.; Havlas, Z. *Chem. Rev.* **2000**, *100*, 4253.

(2) Barnes, A. J. *J. Mol. Struct*. **2004**, *704*, 3 and references therein.

(3) Grabowski, S. J., Ed. *Hydrogen Bonding − New Insights*; Springer: Dordrecht, The Netherlands, 2006 (see also references therein).

(4) (a) Huggins, M. L. *J. Org. Chem*. **1936**, *1*, 407. (b) Huggins, M. L. *Angew. Chem., Int. Ed. Engl*. **1971**, *10*, 147. (c) Glasstone, S. *Trans. Faraday Soc*. **1937**, *33*, 200. (d) Marvel, C. S.; Harkema, J. H. *J. Am. Chem. Soc*. **1941**, *63*, 1609 and reference therein. (e) Stanford, S. C.; Gordy, W. *J. Am. Chem. Soc*. **1941**, *63*, 1094 and references therein. (f) Allerhand, A.; Schleyer, P. v. R. *J. Am. Chem. Soc*. **1963**, *85*, 1715 and references therein.

(5) (a) Afonin, A. V.; Andriyankov, M. A. *Zh. Org. Khim*. **1988**, *24*, 1034. (b) Satonaka, H.; Abe, K.; Hirota, M. *Bull. Chem. Soc. Jpn*. **1988**, *61*, 2031. (c) Afonin, A. V.; Sigalov, M. V.; Korostova, S. E.; Aliev, I. A.; Vashchenko, A. V.; Trofimov, B. A. *Magn. Reson. Chem*. **1990**, *28*, 580. (d) Afonin, A. V.; Vashchenko, A. V.; Fujiwara, H. *Bull. Chem. Soc. Jpn*. **1996**, *69*, 933.

(6) (a) Desiraju, G. R.; Steiner, T. *The Weak Hydrogen Bond in Structural Chemistry and Biology*; Oxford University Press: Oxford, U.K., 1999. (b) Desiraju, G. R. *Acc. Chem. Res*. **1996**, *29*, 441. (c) Desiraju, G. R. *Chem. Commun*. **2005**, 2995. (d) Martin, T. W.; Derewenda, Z. S. *Nature Structural Biology* **1999**, *6*, 403. (e) Jeffrey, G. A. *J. Mol. Struct*. **1999**, *485−486*, 293. (f) Kryachko, E. S. In *Hydrogen Bonding − New Insights*; Grabowski, S. J., Ed.; Springer: Dordrecht, The Netherlands, 2006; Chapter 8.

(7) Gu, Y.; Kar, T.; Scheiner, S. *J. Am. Chem. Soc*. **1999**, *121*, 9411.

(8) Hobza, P.; Havlas, Z. *Chem. Phys. Lett*. **1999**, *303*, 447.

(9) Kryachko, E. S.; Zeegers-Huyskens, T. *J. Phys. Chem. A* **2001**, *105*, 7118.

(10) Alabugin, I. V.; Manoharan, M.; Peabody, S.; Weinhold, F. *J. Am. Chem. Soc*. **2003**, *125*, 5973.

(11) Pejov, L.; Hermansson, K. *J. Chem. Phys*. **2003**, *119*, 313.

(12) Li, X.; Liu, L.; Schlegel, H. B. *J. Am. Chem. Soc*. **2002**, *124*, 9639.

(13) Masunov, A.; Dannenberg, J. J.; Contreras, R. H. *J. Phys. Chem. A* **2001**, *105*, 4737.

(14) Hermansson, K. *J. Phys. Chem. A* **2002**, *106*, 4695.

(15) Qian, W.; Krimm, S. *J. Phys. Chem. A* **2002**, *106*, 6628.

(16) (a) Karpfen, A.; Kryachko, E. S. *J. Phys. Chem. A* **2005**, *109*, 8930. (b) Karpfen, A. *J. Mol. Struct. (THEOCHEM*) **2005**, *757*, 203.

(17) (a) Karpfen, A.; Kryachko, E. S. *Chem. Phys*. **2005**, *310*, 77. (b) Karpfen, A.; Kryachko, E. S. *J. Phys. Chem. A* **2003**, *107*, 9724.

(18) Karpfen, A. *J. Mol. Struct. (THEOCHEM*) **2004**, *710*, 85.

(19) (a) Kryachko, E. S.; Karpfen, A. *Chem. Phys*. **2006**, *329*, 313. (b) Karpfen, A.; Kryachko, E. S. *Chem. Phys. Lett*. **2006**, *431*, 428.

(20) Reed, A. E.; Schleyer, P. v. R. *J. Am. Chem. Soc*. **1990**, *112*, 1434.

(21) Wiberg, K. B.; Marquez, M.; Castejon, H. *J. Org. Chem*. **1994**, *59*, 6817.

(22) Barnes, A. J.; Beech, T. R. *Chem. Phys. Lett*. **1983**, *94*, 568.

(23) (a) Katsumoto, Y.; Komatsu, H.; Ohno, K. *J. Am. Chem. Soc*. **2006**, *128*, 9278. (b) Xu, Z.; Li, H.; Wang, C. *Chem Phys Chem* **2006**, *7*, 2460. (c) Fu, A. P.; Du, D. M.; Zhou, Z. Y. *Chem. Phys. Lett*. **2003**, *377*, 537. (d) Parreira, R. L. T.; Galembeck, S. E.; Hobza, P. *Chem Phys Chem* **2007**, *8*, 87.

(24) Møller, C.; Plesset, M. S. *Phys. Rev*. **1934**, *46*, 618.

(25) (a) Woon, D. E.; Dunning, Jr., T. H. *J. Chem. Phys*. **1993**, *98*, 1358. (b) Kendall, R. E.; Dunning, T. H., Jr.; Harrison, R. J. *J. Chem. Phys*. **1992**, *96*, 6796.

(26) Frisch, M. J.; Trucks, G. W.; Schlegel, H. B.; Scuseria, G. E.; Robb, M. A.; Cheeseman, J. R.; Montgomery, J. A., Jr.; Vreven, T.; Kudin, K. N.; Burant, J. C.; Millam, J. M.; Iyengar, S. S.; Tomasi, J.; Barone, V.; Mennucci, B.; Cossi, M.; Scalmani, G.; Rega, N.; Petersson, G. A.; Nakatsuji, H.; Hada, M.; Ehara, M.; Toyota, K.; Fukuda, R.; Hasegawa, J.; Ishida, M.; Nakajima, T.; Honda, Y.; Kitao, O.; Nakai, H.; Klene, M.; Li, X.; Knox, J. E.; Hratchian, H. P.; Cross, J. B.; Bakken, V.; Adamo, C.; Jaramillo, J.; Gomperts, R.; Stratmann, R. E.; Yazyev, O.; Austin, A. J.; Cammi, R.; Pomelli, C.; Ochterski, J. W.; Ayala, P. Y.; Morokuma, K.; Voth, G. A.; Salvador, P.; Dannenberg, J. J.; Zakrzewski, V. G.; Dapprich, S.; Daniels, A. D.; Strain, M. C.; Farkas, O.; Malick, D. K.; Rabuck, A. D.; Raghavachari, K.; Foresman, J. B.; Ortiz, J. V.; Cui, Q.; Baboul, A. G.; Clifford, S.; Cioslowski, J.; Stefanov, B. B.; Liu, G.; Liashenko, A.; Piskorz, P.; Komaromi, I.; Martin, R. L.; Fox, D. J.; Keith, T.; Al-Laham, M. A.; Peng, C. Y.; Nanayakkara, A.; Challacombe, M.; Gill, P. M. W.; Johnson, B.; Chen, W.; Wong, M. W.; Gonzalez, C.; Pople, J. A. *Gaussian 03*, revision C.02; Gaussian, Inc.: Wallingford, CT, 2004.

(27) Martin, J. M. L.; Van Alsenoy, C. *GAR2PED Program*; University of Antwerp: Antwerpen, 1995.

(28) (a) Bock, W. B.; Trachtman, M.; George, P. *J. Comput. Chem*. **1981**, *2*, 30. (b) Wiberg, K. B.; Hadad, C. M.; Rablen, P. R.; Cioslowsky, J. *J. Am. Chem. Soc*. **1992**, *114*, 8644. (c) Ssász, G.; Borisenko, K. B.; Hargittai, I. *J. Mol. Struct. (THEOCHEM*) **1997**, *393*, 111. (d) Wiberg, K. B. *Acc. Chem. Res*. **1999**, *32*, 922.

(29) (a) Pereira, A.; Coitino, E. L.: Ventura, O. N. *J. Mol. Struct. (THEOCHEM*) **1994**, *314*, 31. (b) Koch, U.; Egert, E. *J. Comp. Chem*. **1995**, *16*, 937. (c) Platts, J. A.; Howard, S. T.; Bracke, B. R. F. *J. Am. Chem. Soc*. **1996**, *118*, 2726. (d) Del Bene, J. E.; Gwaltney, S. R.; Bartlett, R. J. *J. Phys. Chem. A* **1998**, *102*, 5124. (e) Salai Cheettu Ammal, S.; Venuvanalingam, P. *J. Phys. Chem. A* **2000**, *104*, 10859. (f) Popelier, P. J. A.; Houbert, L.; Kosov, D. S. *J. Phys. Chem. A* **2001**, *105*, 8254.

(30) (a) Del Bene, J. E. *J. Am. Chem. Soc*. **1973**, *95*, 6517. (b) Ventura, O. N.; Coitino, E. L.; Lledos, A. *J. Comput. Chem*. **1992**, *13*, 1037. (c) Kumpf, R. A.; Damewood, J. R., Jr. *J. Phys. Chem*. **1989**, *93*, 4478. (d) Dimitrova, Y.; Peyerimhoff, S. D. *Chem. Phys. Lett*. **1994**, *227*, 384. (e) Ramelot, T. A.; Hu, C.-H.; Fowler, J. E.; DeLeeuw, B. J.; Schaefer, H. F., III. *J. Chem. Phys*. **1994**, *100*, 4347. (f) Masella, M.; Flament, J.-P. *J. Chem. Phys*. **1999**, *110*, 7245.

(31) (a) Nowek, A.; Leszczynski, J. *Int. J. Quantum Chem*. **1996**, *57*, 757. (b) Bobadova-Parmanova, P.; Galabov, P. *J. Phys. Chem. A* **1998**, *102*, 1815. (c) Galabov, P.; Bobadova-Parmanova, P. P. *J. Phys. Chem. A* **1999**, *103*, 5793. (d) Gadre, S. R.; Bhadane, B. K. *J. Phys. Chem. A* **1999**, *103*, 3512.

(32) (a) Francisco, J. S.; Williams, I. H. *J. Am. Chem. Soc*. **1993**, *115*, 3746. (b) Chandra, A. K.; Nguyen, M. T.; Zeegers-Huyskens, T. *Chem. Phys*. **2000**, *255*, 149.

(33) Karpfen, A. *Adv. Chem. Phys*. **2002**, *123*, 469 and references therein.

(34) In this context it is, however, important to note that a sharp definition of non-additivity is hardly possible for *mixed* cyclic clusters because, strictly taken, one would have to search for a second minimum of the mixed dimer, i.e., the HRCO−HF or HRCO−H_2O dimer with a H-F···H-C or H-O···H-C hydrogen bond. The latter is not a stationary structure for most cases. Consequently, the explicit calculation of three-body contributions has been omitted in this work.

(35) (a) Karpfen, A. *Int. J. Quantum Chem Symp*. **1990**, *24*, 129. (b) Karpfen, A. In *Molecular Interactions − From van der Waals to Strongly Bound Complexes*; Scheiner, S., Ed.; Wiley: Chichester, U.K., 1997; p 265.

(36) Kar, T.; Scheiner, S. *J. Phys. Chem. A* **2004**, *108*, 9161.

(37) Karpfen, A.; Schuster, P. *Can. J. Chem*. **1985**, *63*, 809.

(38) Suhai, S. *J. Chem. Phys*. **1994**, *101*, 9766.

(39) (a) Karpfen, A. *Chem. Phys*. **1983**, *79*, 211. (b) Karpfen, A. *J. Phys. Chem*. **1996**, *100*, 13474.

(40) Schuster, P., Zundel, G., Sandorfy, C., Eds. *The Hydrogen Bond. Recent Developments in Theory and Experiments*; North-Holland: Amsterdam 1976. *Developments in Theory and Experiments*; North-Holland: Amsterdam, 1976.

(41) (a) Nguyen, H. M. T.; Nguyen, M. T.; Peeters, J.; Zeegers-Huyskens, T. *J. Phys. Chem. A* **2004**, *108*, 11101. (b) Nguyen, H. M. T.; Peeters, J.; Zeegers-Huyskens, T. *J. Mol. Struct*. **2006**, *792*, 16.

(42) Li, A. Y. *J. Chem. Phys*. **2007**, *126*, 154102.